J. Fluid Mech. (1977), *vol.* 81, *part* 2, *pp.* 273–294
Printed in Great Britain

Viscous flow in collapsible tubes of slowly varying elliptical cross-section

By ROSEMARY WILD, T. J. PEDLEY
Department of Applied Mathematics and Theoretical Physics, University of Cambridge
AND D. S. RILEY
Department of Mathematics, University of Southampton, England

(Received 19 November 1976)

This paper is concerned with steady flow in collapsible tubes, such as veins, at fairly low Reynolds number. Lubrication theory is used to calculate the velocity and pressure distribution in an elliptical tube whose cross-sectional area and eccentricity vary slowly and in a given way with longitudinal distance x. The transverse velocity field and the effect of inertia on the primary velocity and pressure distributions are calculated to first order in the relevant small parameter. The results of these calculations are combined with a relationship between transmural pressure and the cross-sectional area at any x which is close to that measured in (large) veins, and are used to predict the pressure and flow in a collapsible tube when a given distribution of external pressure is applied. Different relationships between the tube perimeter and cross-sectional area are examined. The theory is applied to an experiment in which a segment of collapsible tube is supported between two rigid segments, and squeezed; predictions of the relationship between the pressure drop and flow rate are made for various experimental conditions. In particular, when the resistance of the downstream rigid segment is held constant, a range of flow rates is found in which the pressure drop falls as the flow rate is raised; this agrees with experiment.

1. Introduction

The mean blood pressure in the systemic arteries of most mammals is about 13 kN m^{-2} (100 mm Hg) above atmospheric at the level of the heart. As a result of the hydrostatic gradient, this figure is almost doubled in the arteries of the feet of an upright man, and reduced to about 4 kN m^{-2} in those of the hand if it is held above the head. The pressure outside the arteries, in the tissue, is close to atmospheric (in fact about 0·25 kN m^{-2} below, see Wiederhielm (1972); pressures within the chest may vary by $\pm$ 3 kN m^{-2} as a result of respiratory manoeuvres). Thus the transmural pressure $\hat{p}_{\mathrm{tm}}$, tending to distend the vessel, is well above zero for all systemic arteries. Experiments both within and outside the body show that the cross-sections of the systemic arteries are circular over this range of transmural pressures, but show markedly nonlinear elastic properties in that the distensibility

$$D = \hat{A}^{-1} d\hat{A}/d\hat{p}_{\mathrm{tm}}, \tag{1.1}$$

where $\hat{A}$ is the cross-sectional area, increases with transmural pressure. This is

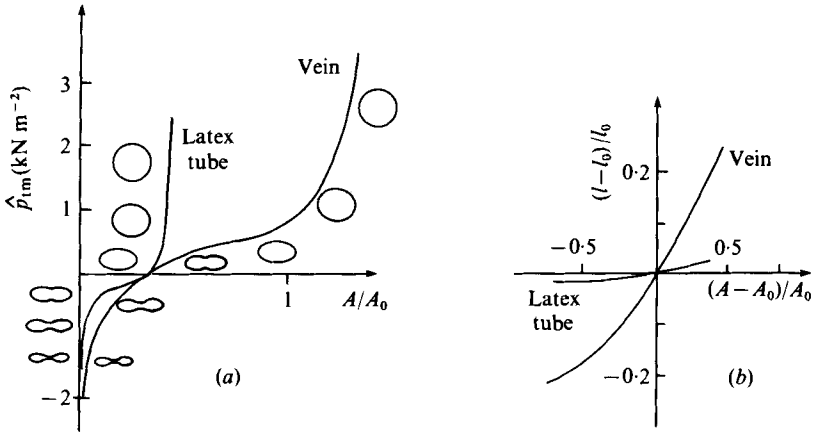

FIGURE 1. Comparison of the elastic properties of a latex tube with those of an excised segment of a canine *vena cava*. (*a*) Transmural pressure as a function of area A, scaled with respect to the area A_0 at zero transmural pressure. Transverse cross-sections are shown for various areas. (*b*) Perimeter as a function of cross-sectional area (Moreno *et al.* 1970, figure 10).

primarily a consequence of the way the elastin and collagen fibres are linked in the wall: at transmural pressures below about 13 kN m^{-2} most of the stress is borne by the elastin fibres (nonlinear material of Young's modulus $E \approx$ 300–800 kN m^{-2}: Carton, Dainauskas & Clark 1962) while at higher values of $\hat{p}_{tm}$ the collagen fibres ($E \approx 10^6$ kN m^{-2}: Benedict, Walker & Harris 1968) become fully extended and increasingly bear the stress.

However, when the transmural pressure of an artery is reduced below about 2kN m^{-2}, for example by the inflation of a cuff around a limb or by the tightening of a tourniquet, the cross-sectional shape changes, becoming increasingly elliptical, and the distensibility also increases. At large negative (i.e. compressive) transmural pressures the cross-section is collapsed into a dumb-bell shape (cf. figure 1) whose inner area is more-or-less completely occluded by corrugations on the endothelial cells. The distensibility has once more become very low because negative cross-sectional areas are impossible.

The elastic properties of systemic arteries at small or negative transmural pressures have not been extensively studied because such pressures are not met in normal physiological conditions. In veins, however, small and negative transmural pressures are commonly experienced, and collapsed veins occur normally, for example in a raised arm. The mean internal pressure in large veins at the level of the heart is about 0·7 kN m^{-2}, so at that level the transmural pressure is just positive. In the foot the internal pressure may therefore be above 10 kN m^{-2} and $\hat{p}_{tm}$ will also be large, but in any vein above the level of the heart the transmural pressure normally beomes subatmospheric and the vessel collapses. The pressure external to veins in the limbs can be increased by muscular action, thereby preventing too great a distension of veins well below the heart, but it cannot be reduced to prevent collapse. (This is not true for veins within the skull, which is a constant-volume chamber; a reduction in blood-vessel volume generates a negative external pressure, preventing further collapse.)

Figure 1 (*a*) shows the cross-sectional area of an excised segment of the *vena cava* of a dog, plotted against transmural pressure (from Moreno *et al.* 1970). At transmural

pressures greater than about 1·5 kN m^{-2} the cross-section of the vein is circular, and the wall is very stiff: stiffer in fact than arteries at the same $\hat{p}_{tm}$, despite the fact that the wall is much thinner, because the collagen within it becomes fully extended at lower transmural pressure than in arteries. Changes in cross-sectional area are accompanied by corresponding changes in perimeter (Attinger 1969). As $\hat{p}_{tm}$ is reduced from 1·5 to 1·0 kN m^{-2}, the vessel still remains circular, but becomes somewhat more distensible, presumably because the elastin in the wall takes over from the collagen. When $\hat{p}_{tm}$ falls below about 1·0 kN m^{-2}, the vessel becomes elliptical, the area falls more rapidly and the distensibility rises. The perimeter also continues to fall, although no longer as the square root of area, and it is this reduction in perimeter, not the change in cross-sectional shape, which makes the larger contribution to the reduction in area (and hence to the rise in distensibility) at least while $\hat{p}_{tm}$ exceeds about 0·5 kN m^{-2}. As $\hat{p}_{tm}$ falls below this value, however, the change in shape becomes more marked, and makes an increasing contribution to the reduction in area. The distensibility has a maximum when $\hat{p}_{tm}$ is slightly below 0·5 kN m^{-2}: from then on it falls, because it becomes increasingly difficult to bend the vessel wall at its points of maximum curvature. When $\hat{p}_{tm}$ has reached a negative value somewhat below $-1{\cdot}0$ kN m^{-2}, the vessel is almost completely collapsed, and the distensibility is very low. Qualitatively similar curves are obtained for pulmonary arteries (Attinger 1969), which have walls whose thickness is intermediate between those of systemic arteries and veins; they normally experience a mean transmural pressure of about 2 kN m^{-2} and, in rabbits at least, are known to have elliptical cross-sections (Caro 1965). Similar results are expected in systemic arteries, but we know of no experiments in which they have been subjected to negative transmural pressures, since these do not normally occur.

It is instructive to compare the pressure–area curve of a vein with that of a rubber tube, because fluid-mechanical experiments are commonly performed with these in the laboratory. The comparison is shown in figure 1 (*a*), for a rubber tube whose internal diameter at $\hat{p}_{tm} = 1{\cdot}0$ kN m^{-2} and whose wall thickness-to-diameter ratio were chosen to be close to those of a canine *vena cava*. The rubber tube remains circular until the transmural pressure falls almost to zero, then becomes elliptical and later dumb-bell shaped like a vein. However, during collapse, the perimeter of the rubber tube remains almost constant (figure 1*b*), and the area change is associated solely with a change of shape. Furthermore the maximum rate of change of area occurs at a negative value of $\hat{p}_{tm}$ (about $-0{\cdot}25$ kN m^{-2}), whereas that for a vein occurs at a positive value. It can also be seen that the slope of the graph in figure 1 (*a*) changes much less abruptly for a vein than for a rubber tube, because of the continuing change in perimeter. The reason for this difference in elastic properties lies in the fact that the rubber is much more resistant to stretch: its Young's modulus is about $2{\cdot}1 \times 10^3$ kN m^{-2}, while that of a vein is about 40 times smaller.

It is the purpose of this paper to investigate some of the fluid-mechanical consequences of the fact that blood vessels (and rubber tubes) collapse when the transmural pressure becomes small or negative. It will be convenient throughout to think in terms of a particular experiment (figure 2) designed both to illustrate the behaviour of veins and to model the situation in an artery constricted by a blood-pressure-measuring cuff (Conrad 1969; Katz, Chen & Moreno 1969). A segment of flexible tube is supported between two lengths of rigid tube and is contained in a chamber whose pressure $\hat{p}_c$ can be given any chosen value. The upstream and downstream pressures in the rigid tubes

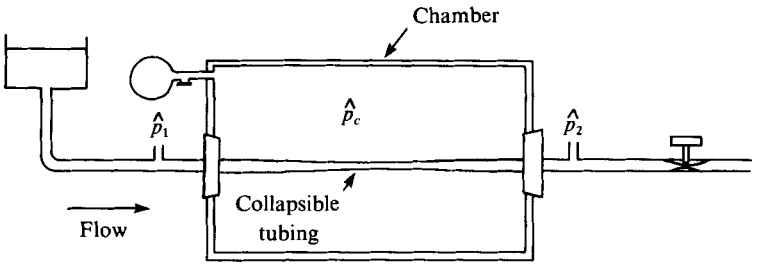

FIGURE 2. Experimental arrangement for studying flow in a collapsible tube.

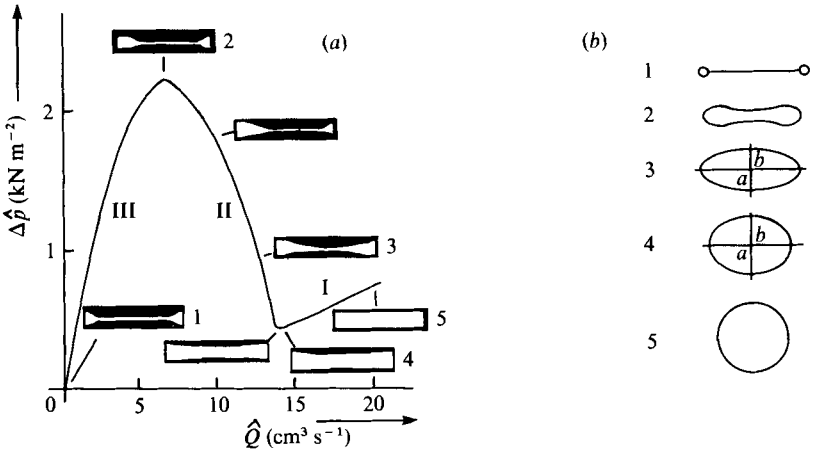

FIGURE 3. (*a*) The pressure drop along the tube as a function of flow rate for fixed downstream resistance and external pressure (Conrad 1969, figure 4*a*). (*b*) Corresponding cross-sections: 1, zero flow; 2, small flow; 3, 4, larger flows; 5, flow so large that tube has become circular.

($\hat{p}_1$ and $\hat{p}_2$) can also be independently controlled. The flow rate $\hat{Q}$ is measured. The results to be described are achieved when the downstream resistance (figure 2) is fixed, when $\hat{p}_c$ is fixed and when $\hat{Q}$ is varied by adjusting the upstream resistance. They are shown as a graph of pressure drop $\hat{p}_1 - \hat{p}_2$ against flow rate $\hat{Q}$ (figure 3) and fall into three distinct categories.

(i) When $\hat{Q}$ is sufficiently large for $\hat{p}_2$ to exceed $\hat{p}_c$, the pressure everywhere in the collapsible segment exceeds $\hat{p}_c$, and the tube remains almost circular; the flow is everywhere Poiseuille flow, so $\hat{p}_1 - \hat{p}_2$ is proportional to $\hat{Q}$, with an almost constant resistance (segment I of figure 3).

(ii) When $\hat{Q}$ is reduced below a certain critical value, the downstream pressure becomes smaller than the chamber pressure. Thus, for a very small further decrease in flow rate, the transmural pressure at the downstream end of the collapsible segment becomes negative, and the cross-section begins to change shape and to collapse. The cross-sectional area falls rapidly as the transmural pressure falls, because of the large distensibility (figure 1*a*), while the flow resistance rises rapidly and the pressure drop required to maintain the (gradually falling) flow rate also rises dramatically (segment II of figure 3). If the downstream resistance is changed during this phase such that $\hat{p}_2$ varies independently of $\hat{p}_1$, very little change in flow rate is observed. However, if

$\hat{p}_e$ is varied instead, the degree to which the tube is collapsed also varies, and the flow rate changes accordingly. In fact, during such manoeuvres the flow rate $\hat{Q}$ is approximately proportional to $\hat{p}_1 - \hat{p}_e$, not $\hat{p}_1 - \hat{p}_2$. In many experiments, self-excited oscillations in area and flow rate are found to develop during this phase, even when the height of the upstream reservoir, the upstream and downstream resistances and the chamber pressure are held fixed. It is oscillations such as these which are thought to be responsible for the Korotkoff sounds, heard when the arteries in the arm are partially occluded by an inflated cuff, and employed in measurement of blood pressure. In large arteries, and in many of the quoted experiments, the mean Reynolds number of the flow is large, and the mechanism for the generation of the oscillations (which is not well understood) is unlikely to involve viscosity as a primary factor. However, no oscillations are observed if the Reynolds number is very small (Fung & Sobin 1972), when viscosity must be important.

(iii) Finally, when the whole segment has collapsed ($\hat{p}_1 < \hat{p}_e$), its cross-section has a rather rigid dumb-bell configuration, and as the flow rate is reduced still further, no further change in cross-section occurs, the resistance once more becoming constant, at a value 10–100 times higher than that before collapse (segment III of figure 3).

It is hoped subsequently to develop the theory for unsteady flow, and to predict a value of the Reynolds number above which oscillations can occur. However, in this paper we restrict consideration to steady flow at fairly low Reynolds numbers, and our results will be directly relevant only to quasi-steady flow in fairly small blood vessels undergoing compression.

The analysis is based on lubrication theory and requires that the cross-sectional area varies slowly with longitudinal distance. The effect of inertia is included as a perturbation to the basic lubrication theory solution, and is included because it is not negligible in the experiments and without inertia self-excited oscillations cannot develop.

The basic solution was first given, and applied to tubes of circular cross-section, by Rubinow & Keller (1972). They showed that the flow rate $\hat{Q}$ and the local pressure gradient $d\hat{p}/d\hat{x}$ are related by an equation of the form

$$\hat{Q} = -\sigma\, d\hat{p}/d\hat{x}, \tag{1.2}$$

where σ is the conductance, which depends on the cross-sectional area (as deduced from lubrication theory) and hence, from data such as that of figure 1 (*a*), on the transmural pressure $\hat{p}_{\mathrm{tm}}$. Now $\hat{p}_{\mathrm{tm}} = \hat{p} - \hat{p}_e$, where $\hat{p}$ is the internal pressure, and $\hat{p}_e$ the external pressure (assumed constant), and $\hat{Q}$ is independent of x. Thus, if L is the distance between the upstream station where $\hat{p} = \hat{p}_1$ and the downstream station where $\hat{p} = \hat{p}_2$, integration of (1.2) gives

$$\hat{Q} = \frac{1}{L}\int_{\hat{p}_2}^{\hat{p}_1} \sigma(\hat{p} - \hat{p}_e)\, d\hat{p}. \tag{1.3}$$

If $\hat{p}_2 > \hat{p}_e$, σ will be fairly large and more or less independent of $\hat{p}$ (because the distensibility is small), so $\hat{Q}$ will be approximately proportional to $\hat{p}_1 - \hat{p}_2$. On the other hand, if $\hat{p}_2 < \hat{p}_e$, σ will be very small for values of $\hat{p}$ less than about $\hat{p}_e$, and (1.3) can be approximately replaced by

$$\hat{Q} \approx \frac{1}{L}\int_{p_e}^{p_1} \sigma(\hat{p} - \hat{p}_e)\, d\hat{p},$$

which is independent of $\hat{p}_2$. This is the explanation of the steady experimental results described above.

The present work extends that of Rubinow & Keller (1972) in four ways. First, we consider tubes of elliptic cross-section, in order more accurately to model their collapse. This model is incorrect when the cross-section becomes dumb-bell shaped and its area very small, but the measured pressure–area relation is rather uncertain then anyway, and a better model would not make the predictions of conductance (which is very low in these circumstances) more accurate. Flaherty, Keller & Rubinow (1972) computed the shape and conductance σ of a buckled cylindrical tube, uniform along its length. Second, we include to first order the effects of inertia, as was done for rigid circular tubes by Manton (1971) as a perturbation to lubrication theory, and by Lee & Fung (1970) numerically. Hall (1974) considered the unsteady flow in a slowly varying rigid tube of small eccentricity when a pulsatile pressure difference is applied across its ends. Third, we do not restrict attention to uniform external pressure $\hat{p}_e$, but calculate the variation in internal pressure, fluid velocity and tube cross-sectional area when the external pressure resembles that applied by a cuff of finite length (see figure 8 below). Fourth, the calculations of Rubinow & Keller (1972) did not cover the experiment described above in which the downstream resistance is held constant. Our results do extend to this case and in fact they are found to predict multiple-valued $\hat{Q}$–$\Delta\hat{p}$ curves like that of figure 3. Like all the quoted authors, we take blood to be a homogeneous and Newtonian fluid, which is a good approximation in vessels of diameter greater than 100 μm, in which the shear rate exceeds 100 s^{-1} (Whitmore 1968).

2. Lubrication theory and the effect of inertia

In steady conditions the shape of the tube does not change with time, and the relationship between the local pressure gradient and flow in an arbitrary slowly varying elliptical tube can be calculated independently of the pressure–area relation.

We consider steady, viscous, incompressible flow through a slowly varying elliptical tube of length L defined in Cartesian co-ordinates $(Lx, a_0 y, a_0 z)$ by

$$y^2/a^2(x) + z^2/b^2(x) = 1, \quad 0 \leqslant x \leqslant 1, \tag{2.1}$$

where a_0 is a characteristic tube radius and $a_0 a$ and $a_0 b$ are the semi-major and semi-minor axes of the elliptical cross-section. The use of lubrication theory requires that

$$\epsilon = a_0/L \ll 1 \tag{2.2}$$

while the Reynolds number $R = U_0 a_0/\nu$ remains $O(1)$ as $\epsilon \to 0$; U_0 is a scale for the axial velocity component. The velocity field $\hat{\mathbf{u}}$ is scaled such that each dimensionless component is $O(1)$, and is taken to be

$$\hat{\mathbf{u}} = U_0(u, \epsilon v, \epsilon w)$$

with pressure

$$\hat{p} = (\rho U_0^2/\epsilon R)\, p. \tag{2.3}$$

It is convenient to work in a co-ordinate system in which the tube cross-section does not vary with x. Accordingly we introduce new transverse co-ordinates

$$\eta = y/a(x), \quad \zeta = z/b(x)$$

so that (2.1) becomes

$$\eta^2 + \zeta^2 = 1, \quad 0 \leqslant x \leqslant 1. \tag{2.4}$$

The full equations of motion are the continuity equation

$$Du+\frac{1}{a}v_\eta+\frac{1}{b}w_\zeta=0, \tag{2.5}$$

the x-momentum equation

$$\epsilon R\left(uDu+\frac{v}{a}u_\eta+\frac{w}{b}u_\zeta\right)=-Dp+\frac{1}{a^2}u_{\eta\eta}+\frac{1}{b^2}u_{\zeta\zeta}+\epsilon^2D^2u, \tag{2.6}$$

the y-momentum equation

$$\epsilon R\left(uDv+\frac{v}{a}v_\eta+\frac{w}{b}v_\zeta\right)=-\frac{1}{\epsilon^2a}p_\eta+\frac{1}{a^2}v_{\zeta\zeta}+\frac{1}{b^2}v_{\eta\eta}+\epsilon^2D^2v \tag{2.7}$$

and the z-momentum equation

$$\epsilon R\left(uDw+\frac{v}{a}w_\eta+\frac{w}{b}w_\zeta\right)=-\frac{1}{\epsilon^2b}p_\zeta+\frac{1}{a^2}w_{\eta\eta}+\frac{1}{b^2}w_{\zeta\zeta}+\epsilon^2D^2w, \tag{2.8}$$

where

$$D=\frac{\partial}{\partial x}-\frac{a'}{a}\eta\frac{\partial}{\partial\eta}-\frac{b'}{b}\zeta\frac{\partial}{\partial\zeta}$$

and a prime means d/dx. The boundary conditions are simply $u=v=w=0$ on the wall (2.4).

We solve the problem as a power series in ϵ, on the assumption that $R=O(1)$. Thus we take

$$u=u_0+\epsilon u_1+\epsilon^2u_2+\ldots,$$

with similar expressions for v, w and p. The leading terms in (2.7) and (2.8) show that p_0 is a function only of x, and the leading term of (2.6) (the equation for unidirectional motion) gives

$$u_0(x,\eta,\zeta)=\frac{a^2b^2}{2(a^2+b^2)}G_0(x)\,(1-\eta^2-\zeta^2),$$

where $G_0(x)=-dp_0/dx$. This is the elliptical-tube version of Poiseuille flow. For given functions $a(x)$ and $b(x)$, G_0 is determined by the condition that the volume flow rate is independent of x. If U_0 is defined as the average velocity of the flow when the tube cross-section S is a circle of radius a_0, and if the volume flow rate is non-dimensionalized with respect to $a_0^2U_0$, we have

$$Q\equiv\iint_S uab\,d\eta\,d\zeta=\pi.$$

Hence

$$G_0=4(a^2+b^2)/a^3b^3 \tag{2.9}$$

and

$$u_0=(2/ab)\,(1-\eta^2-\zeta^2). \tag{2.10}$$

This is the basic lubrication theory solution, leading to a value for the conductance σ [equation (1.2)] of

$$\frac{\pi}{4\mu}\frac{\hat{a}^3\hat{b}^3}{(\hat{a}^2+\hat{b}^2)}.$$

In order to determine the next approximation to u and p it is necessary to calculate

the leading terms v_0 and w_0 of the expansions for the secondary velocities. Equations (2.7) and (2.8) require that these quantities satisfy

$$\frac{1}{a}v_{0\eta\eta\zeta}+\frac{a}{b^2}v_{0\zeta\zeta\zeta}=\frac{b}{a^2}w_{0\eta\eta\eta}+\frac{1}{b}w_{0\eta\zeta\zeta},$$

and (2.5) and (2.10) imply

$$\frac{1}{a}v_{0\eta}+\frac{1}{b}w_{0\zeta}=\frac{2(ab)'}{a^2b^2}(1-\eta^2-\zeta^2)-\frac{4}{ab}\left(\frac{a'}{a}\eta^2+\frac{b'}{b}\zeta^2\right).$$

The solution which satisfies the boundary conditions is

$$v_0=\frac{2a'}{ab}\eta(1-\eta^2-\zeta^2),\quad w_0=\frac{2b'}{ab}\zeta(1-\eta^2-\zeta^2). \tag{2.11}$$

We note that the streamlines of these secondary motions are the same as those of stagnation-point flow as long as a' and b' have opposite signs, since

$$\frac{v_0}{w_0}=\frac{a'\eta}{b'\zeta}=\frac{ya'/a}{zb'/b}.$$

This represents flow out along the major axis and inwards along the minor axis when a is increasing and b decreasing, and vice versa. When a' and b' have the same sign, however, the secondary streamlines are those of a source or sink on the axis $y=z=0$.

The next term in the pressure expansion, p_1, is also independent of η and ζ, from (2.7) and (2.8), so that u_1 satisfies

$$\frac{1}{a^2}u_{1\eta\eta}+\frac{1}{b^2}u_{1\zeta\zeta}=-G_1(x)-\frac{4(ab)'}{a^3b^3}R(1-\eta^2-\zeta^2)^2,$$

where $G_1(x)=-dp_1/dx$. The solution of this which satisfies the boundary condition is

$$u_1=R(1-\eta^2-\zeta^2)(c_0+c_1\eta^2+c_2\eta^4+c_3\zeta^2+c_4\zeta^4+c_5\eta^2\zeta^2), \tag{2.12}$$

where

$$\begin{aligned}
c_0&=\frac{G_1a^2b^2}{2R(a^2+b^2)}+\alpha(33+608\delta^2+2238\delta^4+608\delta^6+33\delta^8),\\
c_1&=-\alpha(66+850\delta^2+1074\delta^4+238\delta^6+12\delta^8),\\
c_2&=+\alpha\beta(33+44\delta^2+3\delta^4),\\
c_3&=-\alpha(12+238\delta^2+1074\delta^4+850\delta^6+66\delta^8),\\
c_4&=+\alpha\beta(3+44\delta^2+33\delta^4),\\
c_5&=4\alpha\beta(3+34\delta^2+3\delta^4)
\end{aligned}$$

and

$$\left.\begin{aligned}
\alpha&=\frac{2b^2A'}{45A^3\beta(1+15\delta^2+15\delta^4+\delta^6)},\\
\beta&=1+6\delta^2+\delta^4,\quad \delta=b/a,\quad A=ab.
\end{aligned}\right\} \tag{2.13), (2.14}$$

G_1 is again determined from the volume flux condition, in the form

$$\iint u_1\,d\eta\,d\zeta=0,$$

which unexpectedly simplifies to

$$G_1(x)=-2RA'/A^3. \tag{2.15}$$

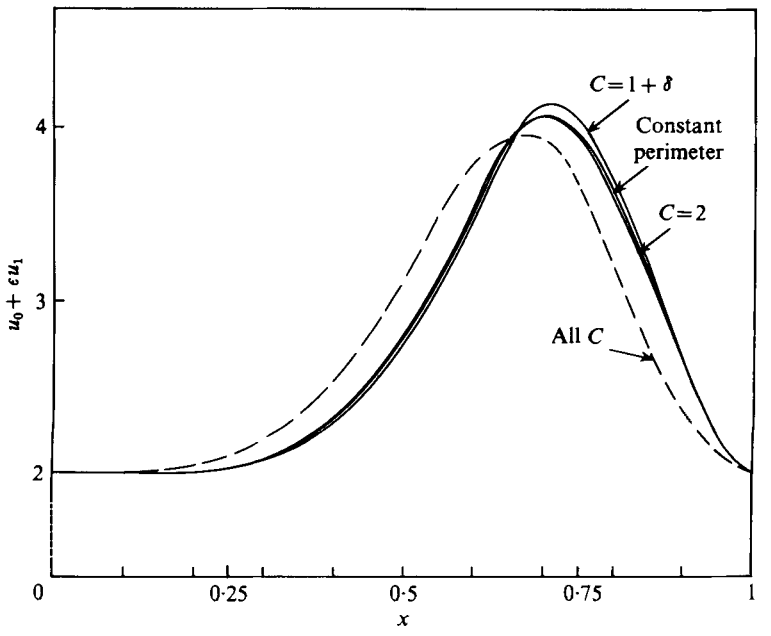

FIGURE 4. The variation of velocity along the centre-line of the rigid tube for three relationships between area and shape (represented by C). – – –, zeroth-order solution ($\epsilon R = 0$); ——, with first-order inertial correction ($\epsilon R = 1$).

Therefore G_1 depends on the area change but not on the cross-sectional shape of the tube. This part of the solution has been expressed in terms of two new variables: δ, which is a measure of the eccentricity of the ellipse and always lies between 0 and 1, and A, the dimensionless cross-sectional area. In the application to elastic tubes it is found convenient to work with these quantities and a mean diameter, represented by

$$C = a+b. \tag{2.16}$$

The effect of inertia on the lubrication solution is expressed by the perturbations ϵu_1 and ϵG_1 to the velocity and pressure gradient. Each term is in fact proportional to ϵR, which is the important small parameter. To see their effect, we look at the velocities and pressure drop in a tube whose elliptical cross-section varies in a given way. The cross-sectional area is taken to vary as

$$A = 1-\tfrac{729}{32}x^4(1-x)^2, \tag{2.17}$$

so that the minimum area of $\frac{1}{2}$ is achieved at $x = \frac{2}{3}$. The shape of the tube is fixed by specifying the relationship between a and b, i.e. between C and δ. Three different relationships are used, as follows:

(i) Constant perimeter (as for rubber tubes) equal to 2π, so that

$$\int_0^{\frac{1}{2}\pi} [1-(1-\delta^2)\sin^2\theta]^{\frac{1}{2}}\,d\theta = \frac{\pi}{2a} = \frac{\pi(1+\delta)}{2C}.$$

(ii) $C = 2$; the perimeter varies by only a small amount when C takes this constant value, equal to its value when the tube is circular with $a = 1$, and this condition is much easier to apply than that of constant perimeter. The difference between the results

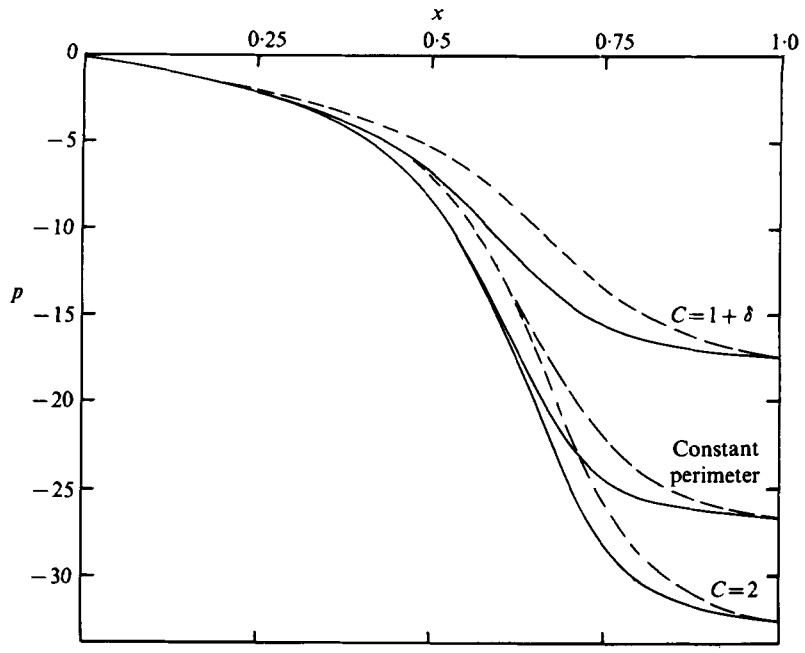

FIGURE 5. The variation of pressure along the centre-line of the rigid tube. – – –, zeroth-order solution ($\epsilon R = 0$); ——, with first-order inertial correction ($\epsilon R = 1$).

obtained from this and from (i) turns out to be small, and (ii) is used in place of (i) in the rest of the paper.

(iii) Perimeter decreasing as area decreases; in view of the limited data, a simple model in which the length of the major axis remains constant as A decreases is chosen to give a qualitative indication of the behaviour of blood vessels. We thus choose

$$C = 1+\delta = 1+A.$$

Results are presented in three ways: the variation of u and p along the centre-line of the tube (figures 4 and 5) and the variation of u_1 across the semi-major and semi-minor axes (figure 6). The constriction in each case accelerates the flow along the centre-line (figure 4) to a maximum velocity which is at $x = \frac{2}{3}$ when inertia is negligible ($\epsilon R = 0$, broken curve), but which increases and occurs further downstream as inertia becomes more important (the solid curves are for $\epsilon R = 1$). The maximum pressure gradient also increases as inertia becomes more important (figure 5), but occurs further upstream than in the absence of inertia, where $A' < 0$ in (2.15). It is interesting to note that the presence of inertia (mediated by the secondary motions) causes a deceleration of the flow in the centre of the tube as A decreases, but an acceleration at the edge on both the major and the minor axis (figure 6). The reverse is true as A increases again. This is in marked contrast with inviscid flow, where the secondary motions cause an acceleration near the wall on the major axis (as A increases) and a deceleration on the minor axis (Sobey 1976). These results also show that there is only a small difference between the constant-perimeter case and the constant-C case, which will therefore be used in its place in future. In the case of constant major axis ($C = 1+\delta$), the perimeter for a given area is smaller than in the other cases. Thus the changes in the velocity and the pressure

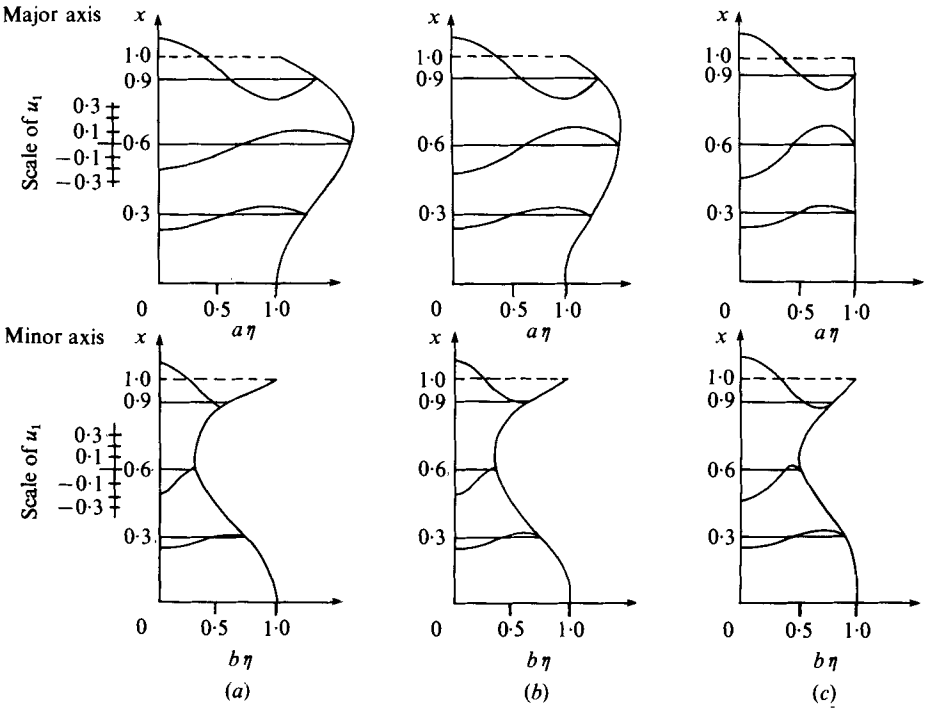

FIGURE 6. First-order velocity profiles at three stations along the semi-major and semi-minor axes of the rigid tube. (*a*) $C = 2$. (*b*) Constant perimeter. (*c*) $C = 1+\delta$.

drop are also significantly smaller, because the cross-section is more nearly circular at each value of A. In this case $v_0 = 0$ [equation (2.11)] and w_0 has the same sign as $b'\zeta$: the secondary streamlines are straight, and parallel to the minor axis.

3. Application to collapsible tubes

In this application the cross-sectional area of the tube at any value of x depends on the local transmural pressure in the manner shown in figure 1 (*a*) and represented by the equation

$$\hat{p}_{\mathrm{tm}} = P_0 F(A), \tag{3.1}$$

where P_0 is a dimensional scaling factor and F is a dimensionless function of A. As before, the area is made dimensionless by dividing by πa_0^2, and now we choose a_0 to be the radius of the tube at the transition between a circular and elliptical cross-section (i.e. the tube is circular for $A \geqslant 1$, elliptical for $A < 1$). We then fix P_0 as the value of $\hat{p}_{\mathrm{tm}}$ when the tube is just circular, i.e. by requiring that $F(1) = 1$. This elastic pressure scale is different from the fluid-dynamic pressure scale used above [equation (2.3)], so we introduce the dimensionless parameter

$$S = \epsilon R P_0/\rho U_0^2 = \pi a_0^4 P_0/\mu L\hat{Q}, \tag{3.2}$$

where $\hat{Q}$ is the flow rate through the tube. Thus, for a given tube with given elastic properties, S can also be regarded as an inverse measure of flow rate. It we stick to the

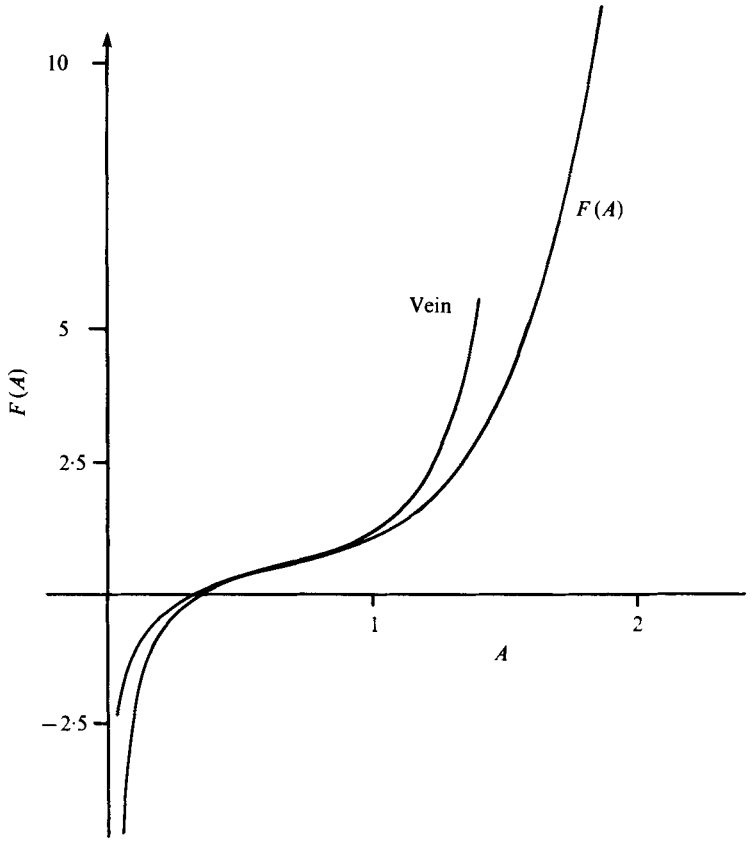

FIGURE 7. Comparison of the function $F(A)$ with the relationship between transmural pressure and area for the canine *vena cava* (as shown in figure 1*a*).

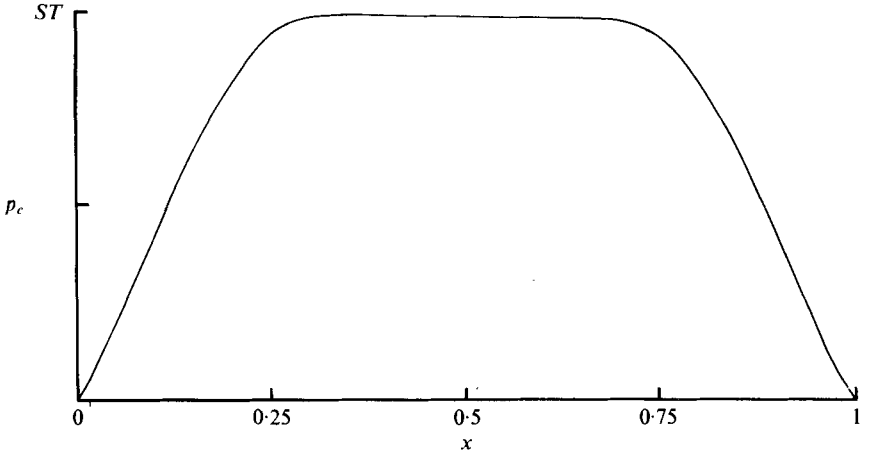

FIGURE 8. The external pressure p_e for an inflated cuff.

convention that all pressures are non-dimensionalized with respect to $\rho U_0^2/\epsilon R$, then (3.1) becomes

$$p_{\mathrm{tm}} = SF(A). \tag{3.1a}$$

The experimental situation we are attempting to model is that of a finite length of collapsible tube with external pressure $(\rho U_0^2/\epsilon R)\, p_e(x)$ given for all x and with internal pressure given at the entrance, $x = 0$. Clearly then, the distribution of area with distance along the tube, and hence the relationship between the pressure drop and the flow rate down the tube, will depend on the transmural pressure at $x = 0$. Thus another dimensionless parameter on which the flow will depend is

$$p_{\mathrm{tm}}(0) = (\rho U_0^2/\epsilon R)\,[\hat{p}(0) - \hat{p}_e(0)];$$

this will determine the initial cross-sectional area $A(0)$, from (3.1a). In computing the results, it is more convenient to specify $A(0)$, and derive $p_{\mathrm{tm}}(0)$ from (3.1a).

For a given flow rate and a given distribution of area, the pressure distribution inside the tube is determined from (2.9) and (2.15). For given distributions of external and internal pressure, the cross-sectional area is determined from (3.1a). Combining the two and using (2.16), we obtain the following ordinary differential equation for $A(x)$:

$$SF'(A)\frac{dA}{dx} = -\frac{dp_e}{dx} - \frac{4(C^2 - 2A)}{A^3} + \frac{2\epsilon R}{A^3}\frac{dA}{dx}. \tag{3.3}$$

This is solved (by simple numerical integration) subject to the initial condition that $A(0)$ is given.

The elastic properties of the tube are represented by the function $F(A)$. This is specified to fit the experimental curve for veins given in figure 1 (a), in the form

$$F(A) = \frac{1}{A}\left[0{\cdot}34(3A-1) + 0{\cdot}01(3A-1)^5 + 0{\cdot}1\frac{(3A-1)}{A^2}e^{-5A}\right]. \tag{3.4}$$

Both curves are plotted in figure 7. The first two terms within the bracket are of the form specified by Rubinow & Keller (1972), and the last term is added to ensure that dA/dx remains finite as $A \to 0$ in (3.3), for otherwise negative areas are predicted and the model breaks down. Note that the area has reduced to one-third of its reference value ($A = \frac{1}{3}$) when the transmural pressure is zero, which is appropriate for veins but not for rubber tubes.

The external pressure p_e could be taken to be constant. Instead we choose a form representative of a cuff inflated over part of the length:

$$p_e(x) = ST[1 - \exp\{1 - 1/4(x - \tfrac{1}{2})^2\}]. \tag{3.5}$$

This is plotted in figure 8; p_e is zero at the two ends of the collapsible segment ($x = 0$ and 1) and takes the maximum value ST at the midpoint $x = \frac{1}{2}$. This corresponds to a dimensional cuff pressure of $\hat{T} = \rho U_0^2 ST/\epsilon R = P_0 T$ [see (3.2)]. Thus, if the flow rate is varied in a given tube with a given cuff pressure, T remains constant as S is varied.

The relationship between the area and the shape of the cross-section must be specified, as in the last section. We shall present results for two cases: one in which $C = 2$ when $A \leqslant 1$ (case (ii) above), which has been shown to give results close to those for

Vein	a_0 (cm)	L (cm)	U_0 (cm s^{-1})	R	ϵR
Inferior *vena cava*	0·5	30	15–40	400–1000	7 –17
Medium-sized vein	0·2	2	1–10	10–100	1 –10
Venule	0·002	0·15	0·2–0·5	0·02–0·05	0·0003–0·0007

TABLE 1. Values of parameters in veins (Caro, Pedley & Seed 1974).

constant perimeter, and one in which the major axis of the ellipse remains constant and the perimeter decreases during collapse [case (iii) above], i.e. in which

$$C = \begin{cases} 2A^{\frac{1}{2}} & \text{for} \quad A \geqslant 1 \text{ (circular)}, \\ 1+A & \text{for} \quad A < 1 \text{ (elliptical)}. \end{cases} \tag{3.6}$$

Integration of (3.3) can proceed when the following parameters have been specified: ϵR, S, T and $A(0)$. The last of these determines $p_{\mathrm{tm}}(0)$ from (3.1a), and this is the same as $p(0)$ because $p_e(0) = 0$. Table 1 gives the radii, lengths, mean velocities, Reynolds numbers and values of ϵR (where ϵ is taken to be the radius–length ratio of the whole vein) for three typical canine veins of different sizes. We can see that the present theory is likely to be inapplicable to large veins, but applicable to medium-sized and small veins where ϵR remains below 2. The pressure–area relation given by (3.4) (and figure 7) was derived for large veins, and is therefore unlikely to be completely accurate when applied to small veins, even when scaled with a different value of A_0, but no further information is available. According to figure 7, P_0 is close to 1·0 kN m^{-2}, and we therefore choose this to be its value. The numbers given in table 1 then show that the parameter S [equation (3.2)] can vary over a very wide range, from about 30 to about 10^4. The results presented below do not cover such a wide range, because they prove to be fairly insensitive to S when S is large since the hydrodynamic pressure drop is then small compared with that required to make a significant change in tube area. T is taken to vary between 0 and 5, at which value the maximum cuff pressure is $5P_0$. The initial area $A(0)$ is taken in turn to be greater than, equal to and less than the area (unity) at which the cross-section begins to become elliptical.

In figure 9 we plot the cross-sectional area A as a function of distance x along the tube for various values of the flow-rate parameter S. The solid curves are with inertia ($\epsilon R = 1$) and the broken curves without ($\epsilon R = 0$). The external pressure is constant ($T = 0{\cdot}5$) and the initial area is also constant ($A(0) = 1{\cdot}1$). Figure 9(a) shows the case of fixed major axis and variable perimeter [equations (3.6)] and figure 9(b) shows the case of approximately constant perimeter ($C = 2$ when $A \leqslant 1$) for comparison. The main feature of the results is that there is a critical flow rate (proportional to S^{-1}) above which the area becomes very small just downstream of the peak external pressure, and does not recover further downstream where the external pressure returns to zero. The critical value of S, say S_0, is about 30 from figure 9(a) and about 40 from figure 9(b). The results are clearly very sensitive to the presence of inertia near this critical flow rate, and predictions which ignore it are likely to be in error. The present predictions are also inaccurate for ϵR as large as 1, when $S \sim S_0$, as can be seen from the large difference between the curves for zero and non-zero inertia, but they do indicate the qualitative effect of inertia. Error is also introduced by the rapid rate of change of A with x, which indicates that the effective value of ϵ may not be very small.

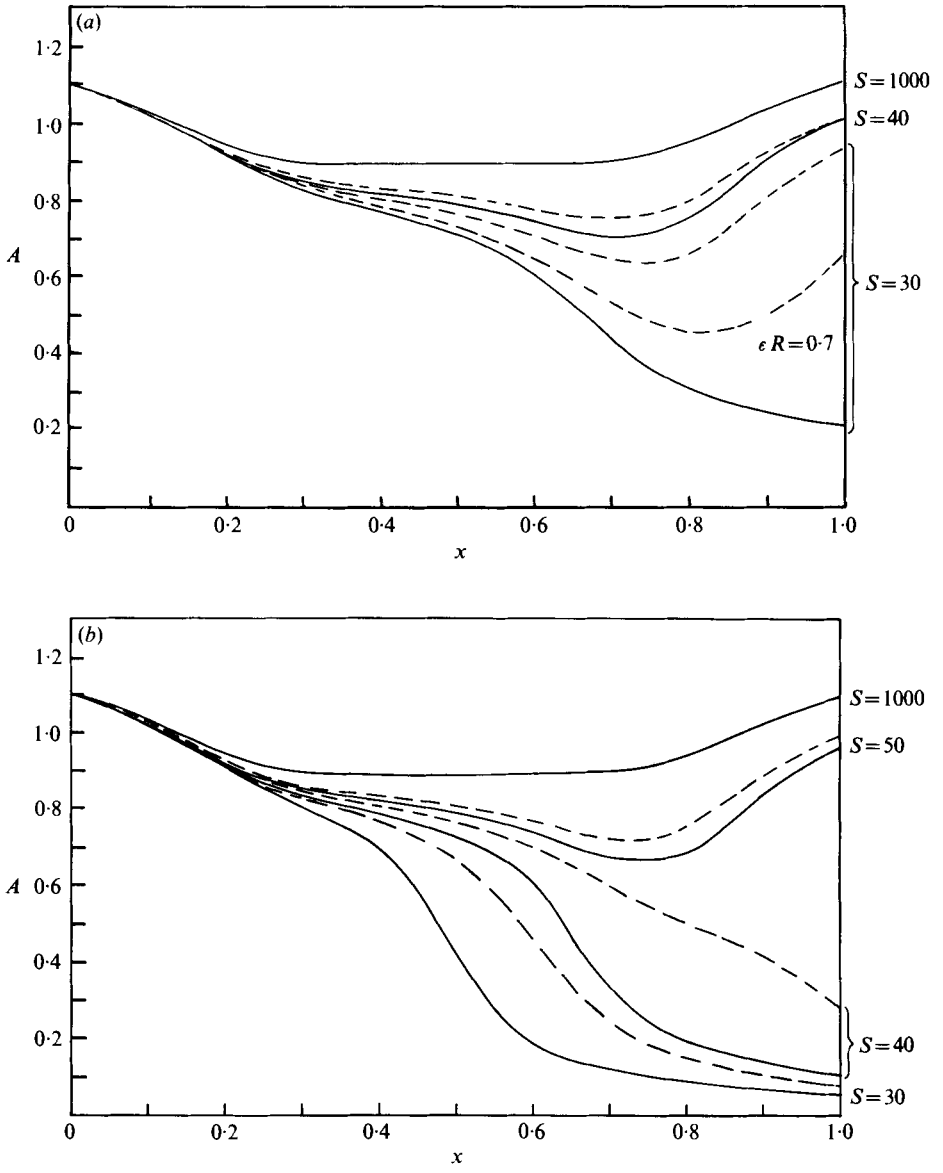

FIGURE 9. Cross-sectional area of the elastic tube as a function of x for various values of the flow-rate parameter S. $C = 2\sqrt{A}$ for $A \geqslant 1$. (*a*) $C = 1 + A$ for $A < 1$. (*b*) $C = 2$ for $A < 1$. – – –, zeroth-order solution ($\epsilon R = 0$); ——, with first-order inertial correction ($\epsilon R = 1$).

It is clear that the pressure drop required for a given flow rate (i.e. the resistance) will be significantly greater for $S < S_0$ than for $S > S_0$. This is confirmed by figure 10, in which the pressure is plotted against x for the cases shown in figure 9.

In figure 11, the area $A(1)$ at the downstream end of the tube is plotted against the external pressure T, again for various values of S and for $\epsilon R = 0, 1$. This indicates how the critical value S_0 increases with T, so that smaller and smaller flow rates are required to generate collapse as T increases. Once more we see that the effect of inertia is small

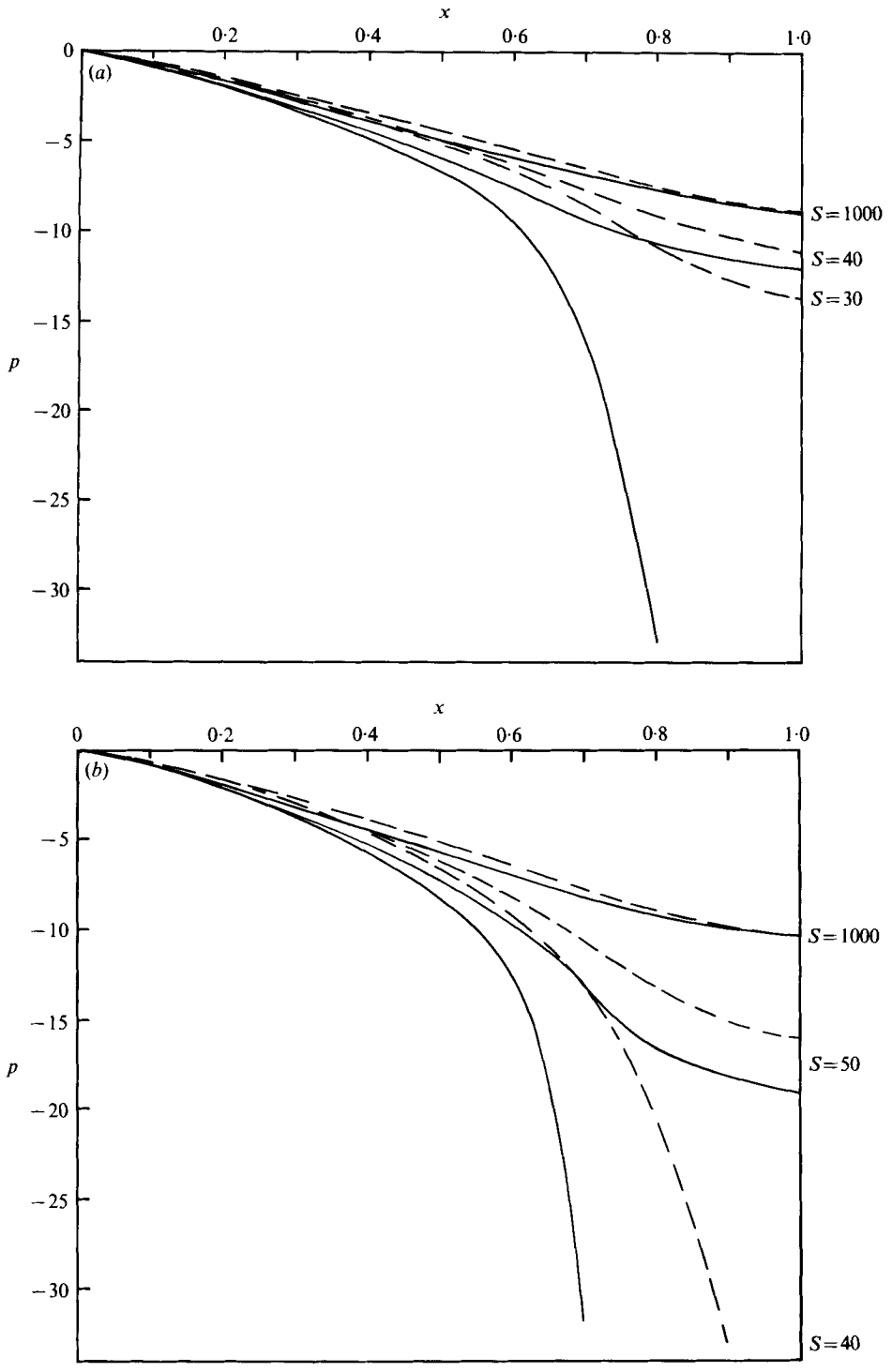

FIGURE 10. The variation of pressure along the centre-line of the elastic tube for various values of S. $C = 2\sqrt{A}$ for $A \geqslant 1$. (*a*) $C = 1+A$ for $A < 1$. (*b*) $C = 2$ for $A < 1$. – – –, $\epsilon R = 0$; ——, $\epsilon R = 1$.

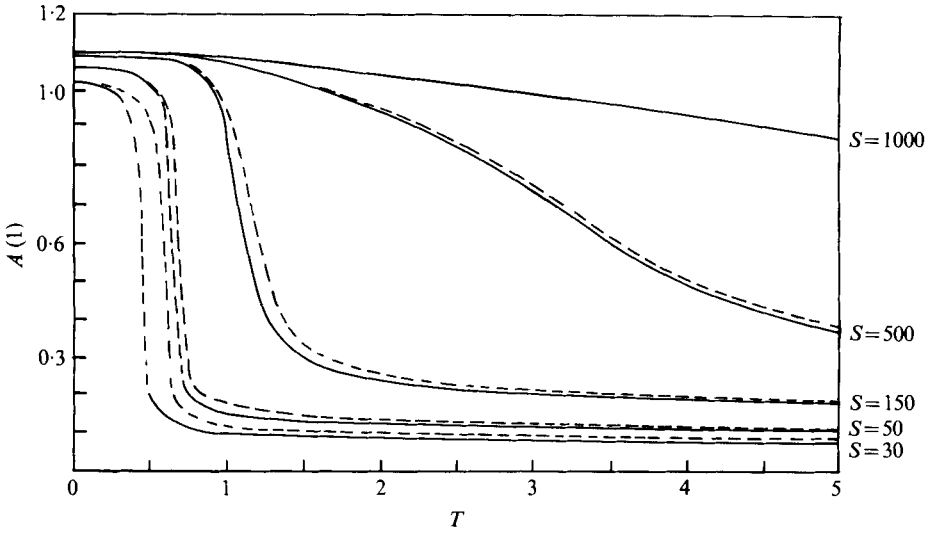

FIGURE 11. Cross-sectional area $A(1)$ at the downstream end of the tube as a function of the external pressure T. Values for S are as for figures 9 and 10. $C = 2\sqrt{A}$ for $A \geqslant 1$; $C = 1+A$ for $A < 1$. – – –, $\epsilon R = 0$; ——, $\epsilon R = 1$; points on the steep gradient have not been computed.

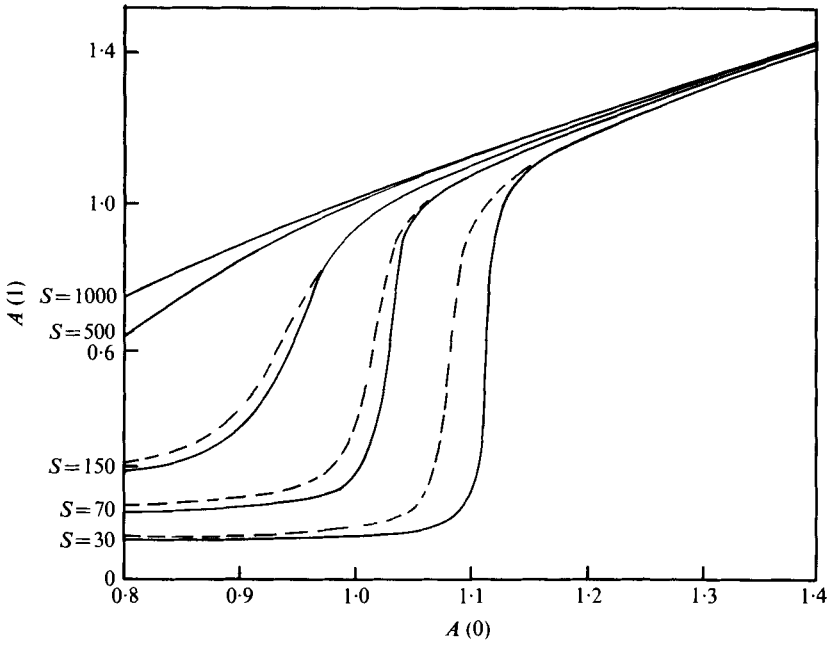

FIGURE 12. Cross-sectional area $A(1)$ at the downstream end of the tube as a function of the initial area $A(0)$. Values of S are as for figures 9 and 10. $C = 2\sqrt{A}$ for $A \geqslant 1$; $C = 1+A$ for $A < 1$. – – –, $\epsilon R = 0$; ——, $\epsilon R = 1$.

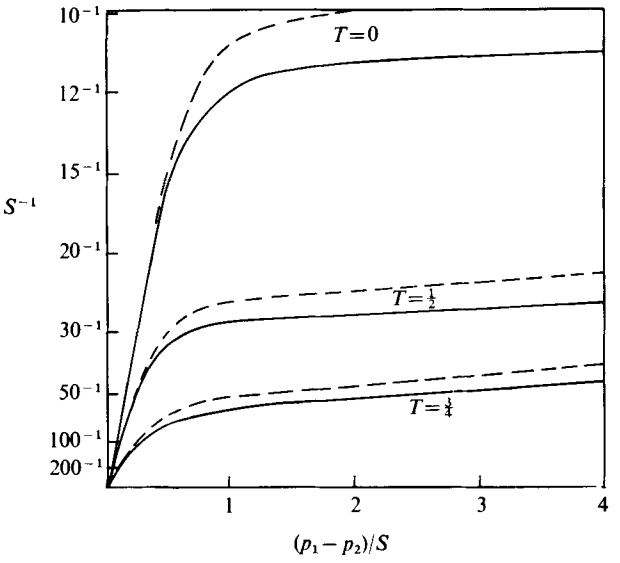

FIGURE 13(*a*). For legend see facing page.

except when S is close to S_0. In figure 12 the same quantity is plotted against the initial area $A(0)$, for a given value of T. Both these figures consider only the case of constant major axis.

In order to make some comparisons with the experiments described in figure 3, we wish to plot the dimensional pressure drop $\hat{p}_1 - \hat{p}_2$ as a function of the flow rate $\hat{Q}$ for given values of the external pressure $\hat{p}_c$ and for given conditions upstream or downstream. In dimensionless terms, this requires that we plot $(p_1 - p_2)/S = (\hat{p}_1 - \hat{p}_2)/P_0$ against S^{-1} for fixed T. Our results for three values of T in conditions where the upstream area $A(0)$ and hence the upstream pressure $\hat{p}(0)$ are held constant are plotted in figure 13(*a*). For these curves, $A(0) = 1{\cdot}1$ and the length of the major axis is held constant, so that the perimeter decreases with area. The point where the curve gradient changes rapidly corresponds approximately to the position of the critical flow rate S_0^{-1} shown in figure 11; this indicates that increases in the driving pressure above a certain critical value do not further increase the flow rate.

These curves are clearly the same shape as those shown in figures 13(*b*) and (*c*), which are redrawn from the work of Brecher (1952) and illustrate his results from experiments on an excised segment of a canine superior *vena cava* (figure 13*c*) and on a rubber tube of comparable dimensions (figure 13*b*). They are also qualitatively similar to the theoretical results obtained by Rubinow & Keller (1972). In order to make quantitative comparisons, we need to estimate the values of the dimensionless constants for Brecher's experiments. He does not give all the necessary data, but we can take the radius of the *vena cava* to be about 0·5 cm (table 1) and suppose a reasonable value of ϵ to be 0·1 (the axial length scale is thus taken to be 5 cm: shorter than the vessel length but possibly an overestimate for a typical length scale during vessel collapse). A flow rate of 4 cm^3 s^{-1} (figure 13*c*) means an average velocity of 5 cm s^{-1}, so when $\nu \simeq 4 \times 10^{-6}$ m^2 s^{-1}, as for blood, the Reynolds number R will be approximately 64 and $\epsilon R \approx 6{\cdot}4$. Furthermore, if we take $P_0 = 1$ kN m^{-2}, as for the *vena cava* in the experiments of

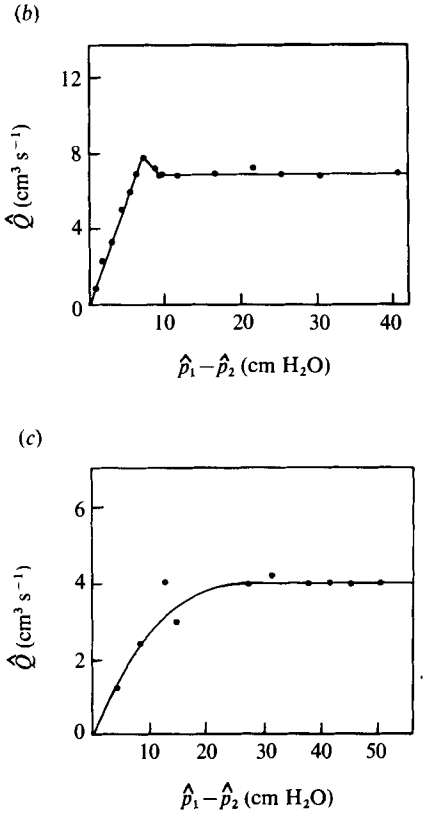

FIGURE 13. (*a*) Predicted pressure drop along the tube as a function of the flow rate S^{-1} for constant upstream area and pressure: – – –, $\epsilon R = 0$; ——, $\epsilon R = 1$. (*b*) Measured pressure drop along a collapsible rubber tube as a function of the flow rate for fixed inlet pressure $\hat{p}_1$ and external pressure $\hat{p}_e$ (measurements of Brecher 1952, as modified by Rubinow & Keller 1972, figure 11). (*c*) Measured pressure drop along the superior *vena cava* of a dog as a function of the flow rate; $\hat{p}_1$ is the pressure in the jugular vein (upstream from the superior *vena cava*) and $\hat{p}_2$ is the pressure applied to the peripheral end (measurements of Brecher 1952, as modified by Rubinow & Keller 1972, figure 10).

Moreno *et al.* (1970) (figure 1), the parameter S is seen to be about 2500. The pressure drops in figure 13(*c*) of 0–50 cm H_2O (i.e. 0–5 kN m^{-2}) are equivalent to values of $(p_1-p_2)/S$ of 0–5. Thus the curve of figure 13(*c*) has a similar abscissa to that of figure 13(*a*), but is squashed down into very small values of the ordinate. The experimental values of T are likely to have been in the neighbourhood of $\frac{3}{4}$ as presumably the external pressure was associated with respiration.

A similar conclusion is reached in the case of Brecher's rubber-tube experiments (figure 13*b*). The value of P_0 was presumably smaller in this case ($P_0 \approx 0{\cdot}2$ kN m^{-2} from figure 1, or $P_0 \approx 0{\cdot}5$ kN m^{-2} from figure 1 of Katz *et al.* 1969), but the flow rates were larger (6 cm^3 s^{-1}) and S will therefore have been nearly as large as for the *vena cava*. The peak in the flow rate on figure 13(*b*) may be explained by the fact that the extent, and hence the resistance, of the collapsed segment increases when $\hat{p}_2$ is reduced below the value at which collapse begins but is still greater than the value (close to $\hat{p}_e$) at which its influence is no longer felt.

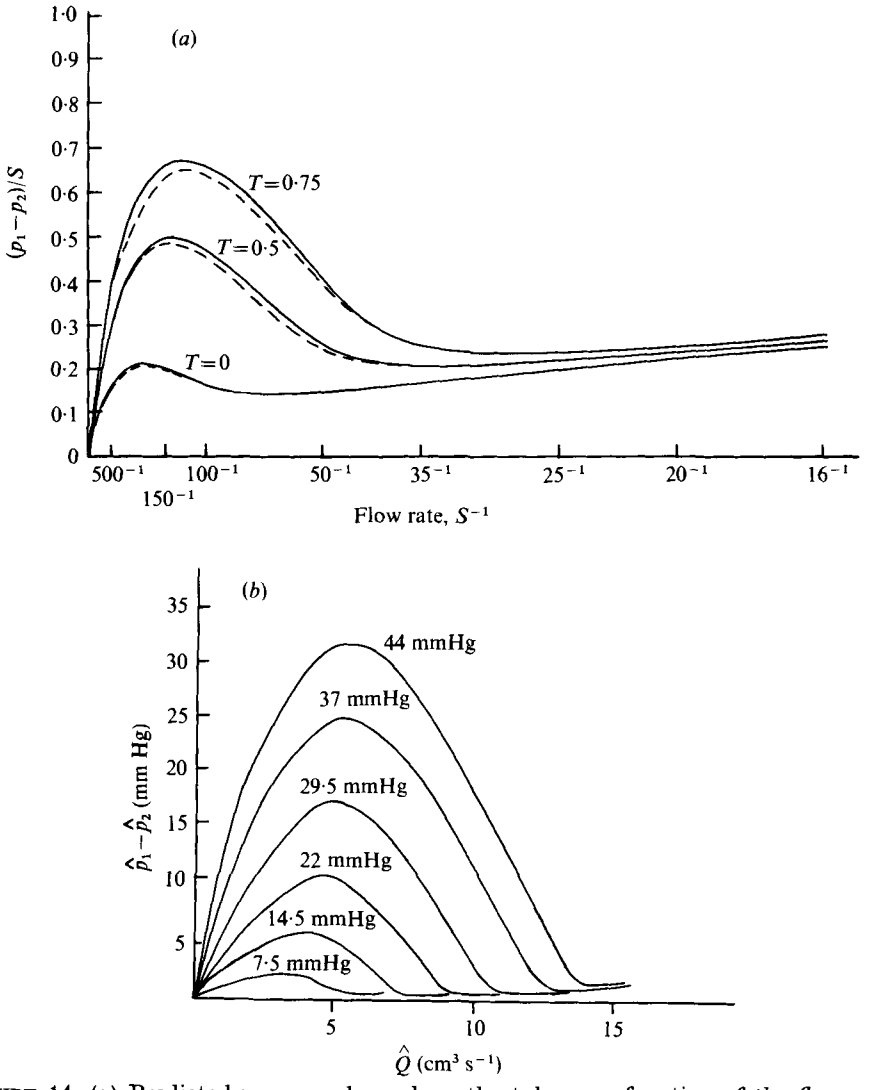

FIGURE 14. (*a*) Predicted pressure drop along the tube as a function of the flow rate S^{-1} for constant downstream resistance. The curves are plotted for T as in figure 13(*a*): – – –, $\epsilon R = 0$; ——, $\epsilon R = \frac{1}{2}$. (*b*) Measured pressure drop along a collapsible tube as a function of the flow rate for constant downstream resistance. The curves are plotted for six external pressures as shown. (Redrawn with curves smoothed from Conrad 1969, figure 5).

The discrepancy in scale between the theoretical and experimental curves must be principally a consequence of the fact that the theory has been developed for $\epsilon R \ll 1$, whilst in the experiments $\epsilon R \approx 6$. Thus the viscous pressure drops in the experiments must have been much less than the dynamic pressure changes experienced by the flow as it passed through the constriction, and the theory cannot be relevant. The fact that the curves have qualitatively the same shape is a consequence of the fact that the constriction causes an enhanced pressure drop at high Reynolds number as well as at low Reynolds number. The mechanism is of course different, probably being associated with separation of the flow from the constriction, rather than enhanced viscous stresses.

If the dynamic pressure drop, instead of the viscous, were used in the non-dimensionalization, the corresponding values of S would be reduced by a factor ϵR, which reduces the estimate of 2500 above to about 400, and therefore puts the experiments and theory on a similar scale.

In figure 14(*a*), we plot the same quantities as in figure 13(*a*), but for a different experiment. This time we keep the downstream resistance R_2 constant as in the experiments of Conrad (1969) which led to figure 3. Constant R_2 means a constant ratio between $\hat{p}_2$ and $\hat{Q}$ or (in dimensionless terms) a constant value of

$$p_2 = \frac{\epsilon \pi a_0^3}{\mu} \frac{\hat{p}_2}{\hat{Q}}.$$

This means that the one-point boundary condition to be applied to (3.3) is that $A(1)$ is given by

$$F[A(1)] = p_2/S$$

for zero external pressure at the downstream end. The higher the flow rate, the higher is S^{-1}, and also $A(1)$, i.e. the collapse is less; integration of (3.3) will determine $A(0)$ and hence p_1. In figure 14(*a*), the constant value of p_2 was taken to be 50, which, when $\epsilon = 0{\cdot}07$ and $a_0 = 0{\cdot}63$ cm, corresponds to a downstream resistance of 91 N m^{-2} per cm^3 s^{-1}, i.e. 6·9 mm Hg per 10 cm^3 s^{-1}, which is comparable with the smallest of the downstream resistances used by Conrad (figure 3*d*). The 'inertial' curves of figure 14(*a*) are for $\epsilon R = 0{\cdot}5$. The main features of this figure are that $\Delta\hat{p}$ is a multiple-valued function of $\hat{Q}$ just as in the experiments, and that this phenomenon is independent of the presence of inertia. As in figure 13(*a*) however, the quantitative comparison is poor because of the large value of S appropriate to the experiments; in Conrad's experiment ($a_0 = 0{\cdot}63$ cm, $P_0 \approx 0{\cdot}5$ kN m^{-2}, $\epsilon = 0{\cdot}07$), a flow rate of 2·5 cm^3 s^{-1} (figure 14*b*) corresponds to $S \approx 10^4$. Once more the discrepancy can be attributed to the dominance of the dynamic pressure drop over the viscous pressure drop in Conrad's high Reynolds number experiments ($\epsilon R \approx 8{\cdot}1$). We know of no experiments that have been performed either on small veins *in situ* or on fairly low Reynolds number flow in collapsible tubes.

When self-excited oscillations occur in collapsible tubes, they do so in the descending section of the curve of pressure drop against flow rate (figure 14*b*). Therefore, in extending the present analysis to the unsteady case, we are currently concentrating on flow rates which fall within the corresponding section of the curves in figure 14(*a*). The aim of this unsteady flow anslysis is to predict a critical value of R above which oscillations can occur.

R.W. and T.J.P. are grateful to the S.R.C. for financial support.

REFERENCES

ATTINGER, E. O. 1969 Wall properties of veins. *I.E.E.E. Trans. Bio-Med. Engng* **16**, 253.

BENEDICT, J. V., WALKER, L. B. & HARRIS, E. H. 1968 Stress–strain characteristics of unembalmed human tendon. *J. Biomech.* **1**, 53.

BRECHER, G. A. 1952 Mechanism of venous flow under different degrees of aspiration. *Am. J. Physiol.* **169**, 423.

CARO, C. G. 1965 Extensibility of blood vessels in isolated rabbit lungs. *J. Physiol.* **178**, 193.

CARO, C. G., PEDLEY, T. J. & SEED, W. A. 1974 Mechanics of the circulation. In *Cardiovascular Physiology* (ed. Guyton & Jones), pp. 1–47. MTP International Review of Science, Physiology, series 1, vol. 1.

CARTON, T. W., DAINAUSKAS, J. & CLARK, J. W. 1962 Elastic properties of single elastin fibres. *J. Appl. Physiol.* **17**, 547.

CONRAD, W. A. 1969 Pressure–flow relationships in collapsible tubes. *I.E.E.E. Trans. Bio-Med. Engng* **16**, 284.

FLAHERTY, J., KELLER, J. B. & RUBINOW, S. I. 1972 Post buckling behaviour of elastic tubes and rings with opposite sides in contact. *SIAM J. Appl. Math.* **23**, 446.

FUNG, Y. C. & SOBIN, S. S. 1972 Pulmonary alveolar blood flow. *Circulation Res.* **30**, 470.

HALL, P. 1974 Unsteady viscous flow in a pipe of slowly-varying cross-section. *J. Fluid Mech.* **64**, 209.

KATZ, A. I., CHEN, Y. & MORENO, A. H. 1969 Flow through a collapsible tube. *Biophys. J.* **9**, 1261.

LEE, J. S. & FUNG, Y. C. 1970 Flow in locally constricted tubes at low Reynolds numbers. *J. Appl. Mech.* E**37**, 9.

MANTON, M. J. 1971 Low Reynolds number flow in slowly varying axisymmetric tubes. *J. Fluid Mech.* **49**, 451.

MORENO, A. H., KATZ, A. I., GOLD, L. D. & REDDY, R. V. 1970 Mechanics of distension of dog veins and other thin-walled structures. *Circulation Res.* **27**, 1069.

RUBINOW, S. I. & KELLER, J. B. 1972 Flow of a viscous fluid through an elastic tube with applications to blood flow. *J. Theor. Biol.* **35**, 299.

SOBEY, I. J. 1976 Inviscid secondary motions in a tube of slowly varying ellipticity. *J. Fluid Mech.* **73**, 621.

WHITMORE, R. L. 1968 *Rheology of the Circulation.* Pergamon.

WIEDERHIELM, C. A. 1972 The interstitial space. In *Biomechanics: Its Foundations and Objectives* (ed. Fung, Perrone & Anliker), pp. 273–286. Prentice-Hall.